



**HAL**  
open science

# Mechanism of large strain accommodation assisted by shear localization in a precipitation-hardened Cu–Be alloy

Ivan Lomakin, Alfia Nigmatullina, Xavier Sauvage

► **To cite this version:**

Ivan Lomakin, Alfia Nigmatullina, Xavier Sauvage. Mechanism of large strain accommodation assisted by shear localization in a precipitation-hardened Cu–Be alloy. *Materials Science and Engineering: A*, 2021, 823, pp.141760. 10.1016/j.msea.2021.141760 . hal-03364713

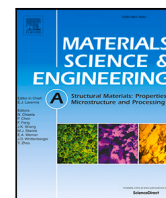
**HAL Id: hal-03364713**

**<https://hal.science/hal-03364713>**

Submitted on 4 Oct 2021

**HAL** is a multi-disciplinary open access archive for the deposit and dissemination of scientific research documents, whether they are published or not. The documents may come from teaching and research institutions in France or abroad, or from public or private research centers.

L'archive ouverte pluridisciplinaire **HAL**, est destinée au dépôt et à la diffusion de documents scientifiques de niveau recherche, publiés ou non, émanant des établissements d'enseignement et de recherche français ou étrangers, des laboratoires publics ou privés.



# Mechanism of large strain accommodation assisted by shear localization in a precipitation-hardened Cu–Be alloy

Ivan Lomakin <sup>a,b,\*</sup>, Alfiya Nigmatullina <sup>a</sup>, Xavier Sauvage <sup>c</sup>

<sup>a</sup> Saint Petersburg University, Laboratory For Mechanics of Bulk Nanostructured Materials, 198504, Saint Petersburg, Russia

<sup>b</sup> Aalto University, Department of Applied Physics, Complex Systems and Materials Group, FI-02150 Espoo, Finland

<sup>c</sup> Normandie Université, UNIROUEN, INSA Rouen, CNRS, Groupe de Physique des Matériaux, 76000, Rouen, France

## ARTICLE INFO

### Keywords:

Copper alloy

Precipitation

Shear band

Strain localization

Ultrafine grains

## ABSTRACT

The influence of the structural state on deformation mechanisms under large strains was investigated in a Cu – 2 wt.% Be alloy. Torque evolutions during straining exhibit serrations typical of structural relaxations in the precipitation-hardened alloy, but not in the solid solution state. Microstructure characterization revealed that homogeneous deformation of the solid solution led to strong grain size reduction (20 nm), while localization occurred in the precipitated state with numerous shear bands. The role of CuBe precipitates on hindering dislocation glide and the resulting shear localization under large strain is discussed.

## 1. Introduction

Dislocation glide is known to be a main mechanism of plastic deformation in crystalline materials [1,2]. Several strategies have been developed to shift the plasticity of materials at higher stresses and tune their mechanical responses. Among these strategies, precipitation hardening relies on the strong interaction between dislocations and nanoscaled precipitates homogeneously nucleated during a so-called precipitation treatment. For example, adding 2 wt% of Be to copper may give rise to a yield stress of up to about 1000 MPa due to the precipitation of CuBe bcc  $\gamma$ -phase [3]. However, this increase in yield stress as compared to commercially pure Cu is accompanied by a significant decrease in ductility. This ductility, evaluated under given stress conditions, is the maximum strain that can be sustained by the material without significant damages that would lead to failure. In some forming processes or under contact conditions, this damage could be delayed due to high hydrostatic pressures, allowing much larger maximum strains to be achieved than those measured in tensile conditions. The mechanisms of plastic deformation and the resulting microstructure evolution in such situation would be rather specific. During the past years, such features have been extensively investigated by severe plastic deformation techniques, for example High Pressure Torsion (HPT). In pure metals or solid solutions, the accumulation of crystalline defects – particularly dislocations – leads to the formation of new grain boundaries, and large strains give rise to ultrafine grain structures [4]. However, the mechanisms occurring in multiphase alloys, especially in the case of precipitation hardening, are not fully understood. Under conventional tensile test conditions, nanoscaled

precipitates could be sheared or by-passed by dislocations; transition between the two mechanisms depends on the precipitate size [5]. Under large strains, however, the accumulation of dislocations loops around the precipitates and may provide new conditions, eventually leading to precipitate shearing. Moreover, mechanical mixing has been reported in a few extreme cases [6,7], thus precipitate dissolution is likely to occur.

To gain new insights into the mechanisms controlling deformation under large strains of alloys hardened by a high density of nanoscaled precipitates, a Cu – 2 wt. % Be alloy was severely deformed up to a total shear strain of 160 under high hydrostatic pressure at room temperature by HPT. The in-situ monitoring of the stress required for severe plastic deformation was combined with a systematic characterization of post-deformation microstructures to highlight the specific mechanisms occurring in the precipitation-treated alloy as compared to the solid solution state.

## 2. Materials and methods

Samples of Cu–2Be in the form of discs (diameter 20 mm, thickness 2 mm) were solubilized at 780 °C for 30 min, then water quenched. Next, half were artificially aged at 325 °C for 10 h to achieve precipitation of CuBe bcc  $\gamma$  nanoscaled particles and a maximum hardening [3]. Severe plastic deformation was introduced by HPT processing at 6 GPa, up to 5 revolutions with a rotation speed of 1 rpm using a Walter Klement GmbH high-pressure torsion press. To monitor the

\* Corresponding author at: Aalto University, Department of Applied Physics, Complex Systems and Materials Group, FI-02150 Espoo, Finland.  
E-mail address: [ivan.lomakin@aalto.fi](mailto:ivan.lomakin@aalto.fi) (I. Lomakin).

<https://doi.org/10.1016/j.msea.2021.141760>

Received 6 April 2021; Received in revised form 13 July 2021; Accepted 14 July 2021

Available online 20 July 2021

0921-5093/© 2021 The Author(s). Published by Elsevier B.V. This is an open access article under the CC BY license (<http://creativecommons.org/licenses/by/4.0/>).

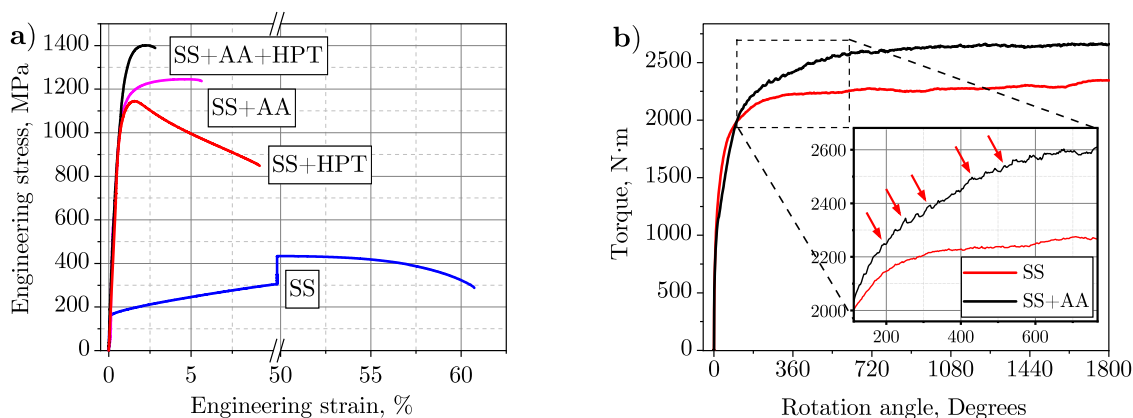


Fig. 1. (a) - engineering stress-strain curves for the Cu-2Be alloy after different thermomechanical treatments. (b) - torque measurements during HPT processing of the Cu-2Be alloy after solid solution (SS) thermal treatment and artificial aging (SS + AA) at 325 °C for 10 h, showing structural relaxations (arrows) of the material.

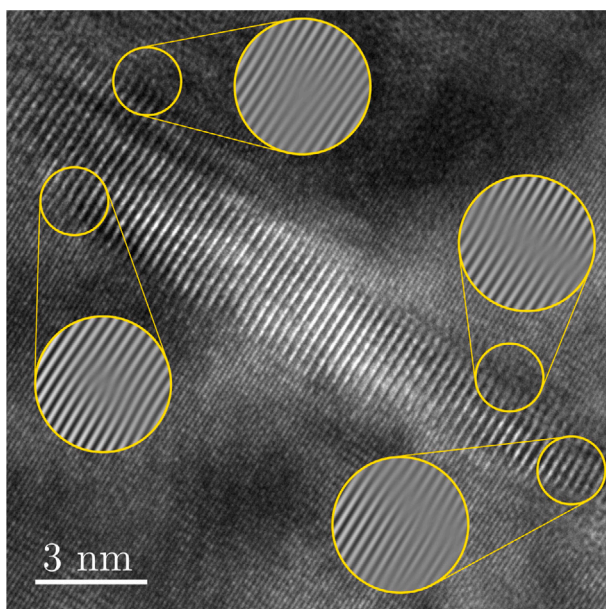


Fig. 2. HRTEM image of the CuBe bcc  $\gamma$ -phase particle in the fcc copper matrix after artificial aging (SS + AA) of the Cu-2Be alloy at 325 °C for 10 h. Inverse Fast Fourier Transform (IFFT) analysis (circled regions) of the particle-matrix interface indicating lattices misfit.

flow stress during deformation, torque measurements were carried out during HPT processing using built-in torque strain gauges connected to a Wheatstone bridge attached to the upper anvil holder. The torque measurement tool was calibrated before each processing procedure.

Phase identification was performed using X-ray diffraction analyses using a Bruker D8 Discover diffractometer ( $\text{CuK}\alpha$  radiation, Bragg's angle 25° to 125° and scanning rate of 5°/min). Microstructures were characterized by scanning electron microscopy (SEM) and transmission electron microscopy (TEM).

SEM specimens were polished and etched with an ammonium persulfate water solution (10 mg of  $(\text{NH}_4)_2\text{S}_2\text{O}_8$  with 100 ml of distilled water) for 60 s to reveal grain boundaries. Images were recorded on a JEOL JSM-7500FA microscope operated at 5 kV, and with an Everhart-Thornley secondary electron detector. TEM specimens were prepared from 3 mm discs cut 5 mm from the center of the HPT samples. After 5 revolutions, this region has sustained a shear strain of  $\gamma \sim 75$  ( $\gamma = 2\pi Nr/h$ , where  $N$  is number of revolutions,  $h$  is thickness of the specimen and  $r$  is the radius). Specimens were first mechanically ground then electropolished using a Struers TenuPol 5

apparatus (electrolyte: 1/3  $\text{HNO}_3$  + 2/3 methanol at -30 °C). The final preparation was carried out using a Gatan PIPS II ion polishing system (acceleration voltage 4 keV). Observations were performed on a JEOL ARM-200F microscope operated at 200 kV. Scanning TEM images were recorded with high-angular annular dark field (HAADF) and dark field detectors (collection angles of 80–180 mrad and 20–80 mrad, respectively).

Stress-strain curves were recorded using a Shimadzu AGX-50 Plus uniaxial tensile test machine at a strain rate of  $5 \cdot 10^{-4} \text{ s}^{-1}$  with samples of  $5.0 \times 2.0 \times 1.0 \text{ mm}$  (details are given in [8]). Specimens were cut out of the HPT samples by electric discharge machining such that the gauge center was located 5 mm from the center of the HPT samples. At least three measurements were carried out for each state to obtain representative data.

### 3. Results and discussion

As expected, the yield stress of the precipitation hardened Cu-2Be alloy is much higher than after the solubilization treatment (130 MPa vs. 1.2 GPa, respectively, Fig. 1a). To reveal the peculiarities of secondary phase interaction with the copper matrix, HRTEM observations were made (Fig. 2). It was found that precipitates are semi-coherent with a copper matrix and crystallographic misfit compensated by a number of dislocations presented on the precipitate-matrix interface. The solubilized Cu-2Be alloy exhibits a significantly larger tensile elongation with a larger strain hardening capability (250 MPa compared to 150 MPa), but the ultimate tensile stress is much lower than for the precipitation-treated alloy (450 MPa vs. 1245 MPa, Fig. 1a). In spite of these significant differences, the torque curves recorded during the severe plastic deformation by HPT are rather similar (Fig. 1b). After two rotations (720°), it seems that a steady state is reached for both materials; the torque saturates at about 2280 and 2650 N m for solubilized and precipitation-hardened alloys, respectively. This 20% difference is consistent with the 20% difference in yield stress measured after HPT (Fig. 1a). Indeed, this type of saturation is quite typical for metallic alloys processed by SPD [4]. However, serrations characterized by avalanche-like drops of the torque are clearly exhibited on the curve of the precipitation-hardened alloy. They do not appear for the solubilized alloy, and indicate some specific structural relaxations during straining. It is well known that some mechanical instabilities may occur during plastic deformation, such as the Portevin-Le Chatelier effect [9] that results from macroscopic localized shear banding due to dynamic aging provided by deformation. Similar strain localization behavior was previously observed both experimentally [10] and as an outcome of simulation [11] over aluminum processed by equal channel angular pressing (ECAP). SEM observations were carried out on as-processed materials to clarify the origin of torque instabilities during HPT.

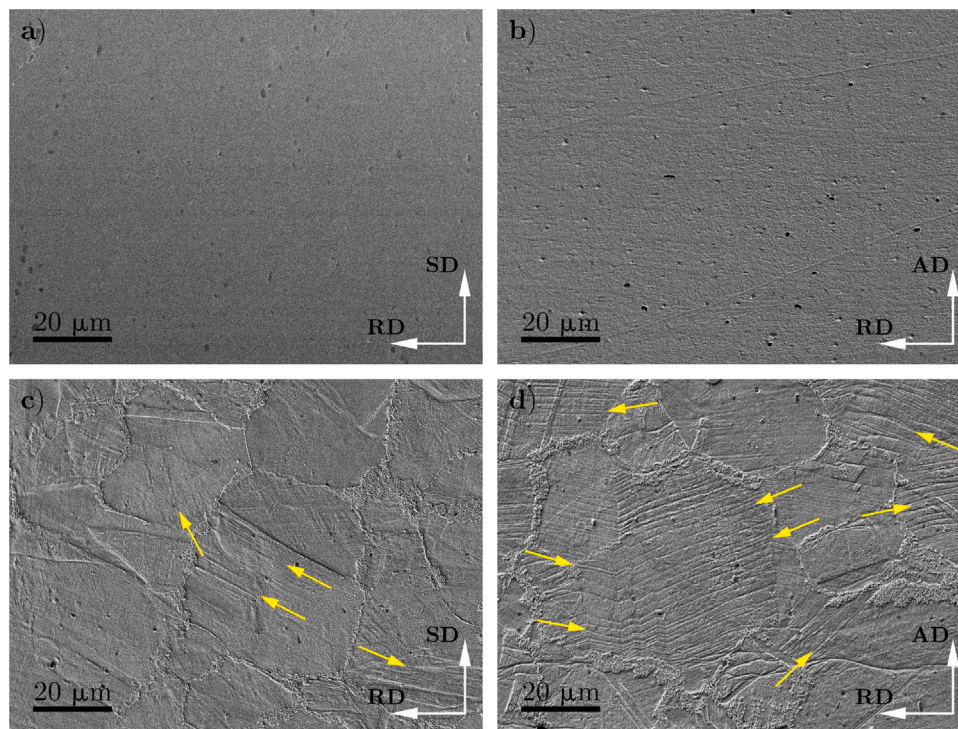


**Fig. 3.** SEM images of the plane surface (a, c) and cross section (b, d), taken 5 mm from the center of the HPT-processed specimens. (a, b) — solubilization treatment with subsequent HPT; (c, d) — artificial aging with subsequent HPT. RD — radial direction, SD — shear direction, AD — axial direction.

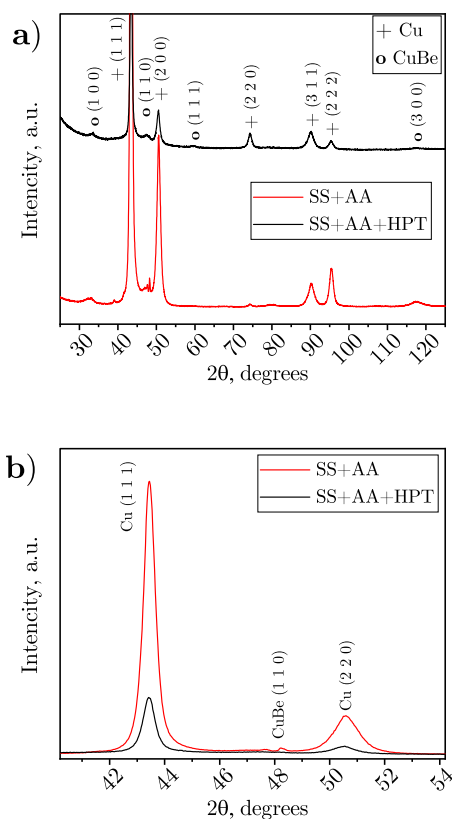


**Fig. 4.** (a) - XRD patterns of the Cu-2Be alloy after different thermomechanical treatments combining solid solution treatment (SS), artificial aging (AA) and severe plastic deformation (HPT). (b) - Enlarged XRD patterns in the range of 40 and 54 degrees.

As revealed by [Fig. 3](#), large differences can be noticed: images of the solubilized alloy (SS + HPT) are featureless, with only a few relatively coarse particles (about 1  $\mu\text{m}$ ) that result from the imperfect etching procedure ([Fig. 3a, b](#)). These observations are consistent with a strong grain refinement induced by SPD [[3](#)]. On the other hand, the precipitation-hardened alloy (AA + HPT) exhibits coarse grains (about 20  $\mu\text{m}$ ) both in plane-view ([Fig. 3c](#)) and cross-section ([Fig. 3d](#)) of the HPT disc, indicating that no grain refinement occurred during SPD. This result is rather unusual for a severely deformed metallic alloy [[4](#)]. There are, however, numerous linear features (arrows on [Fig. 3c](#) and [d](#)) with a much higher density on the cross-sectional view ([Fig. 3d](#)). As the main shear direction (SD) is orthogonal to this surface, these lines might be attributed to localized shear events. This explains the higher amount of observed bands in the cross-section surface compared to the plane-view surface. Microstructural features along grain boundaries and at triple junctions are clusters of discontinuous precipitation in Cu-Be alloys [[12](#)]. X-ray diffraction measurements ([Fig. 4](#)) confirm that relatively little microstructural changes occurred under the large strain imposed by SPD, as both phases (fcc Cu and  $\gamma$  CuBe) are still detected after HPT. Before processing, peaks are relatively broad because of elastic strains necessary for accommodating the misfit between the two phases [[3](#)]. The peak width remains relatively constant during HPT, indicating that a high level of internal stresses is maintained. It is important to note that the relative intensity of Cu peaks has changed, indicating some texture change during HPT, thus proving that the material was effectively strained.

TEM observations were made to confirm and clarify the very different behavior of the Cu-2Be alloy in solid solution and precipitate-hardened states under large strain. In agreement with our earlier study [[3](#)], a nanoscaled structure with a mean grain size of about 20 nm is exhibited in the as-processed solubilized alloy ([Fig. 5a](#)). Note that here we show the image at lower magnification in order to emphasize the visibility of the dramatic differences in microstructures. These observations are also consistent with the significant hardening induced by HPT, leading to an increase in yield stress of up to 1 GPa

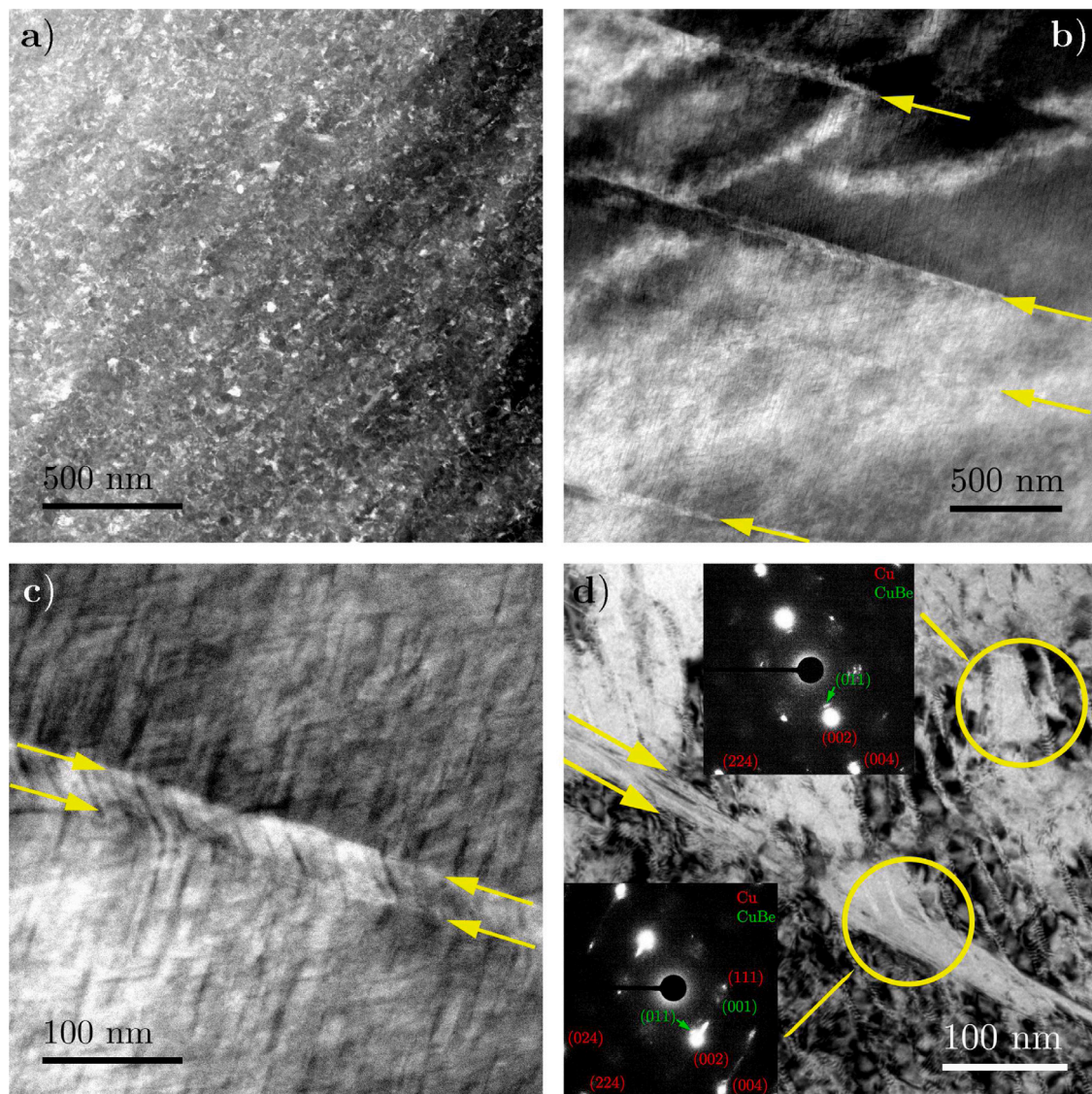


**Fig. 5.** TEM images of the Cu-2Be alloy subjected to solubilization (a) and artificial aging (b–d) prior to HPT. (a) STEM DF images of the Cu-2Be alloy, processed by HPT after the solubilization treatment; (b) STEM DF image at low magnification showing shear bands (arrows); (c) STEM HAADF image of shear band (arrows); (d) TEM BF image corresponding to (c) and SAED patterns recorded in the circled areas.

(Fig. 1a). The situation is however very different in the precipitation-hardened state (Fig. 5b), where grains are still in the micrometer range, in agreement with the SEM observations (Fig. 3). The bright field TEM image (Fig. 5d) exhibits very strong contrast variations, indicating that the copper matrix sustains large elastic strains, partly due to the misfit accommodation between precipitates and the matrix, but also to a high density of dislocation introduced during SPD. Planar features intersecting grains clearly appear (arrows on Fig. 5b, c, d), which are thin bands with a mean apparent thickness of about 50 nm. The typical plate-shaped  $\gamma$ -CuBe precipitates nucleated during the precipitation treatment [3,13,14] are detected on SAED patterns (Fig. 5d), and remain homogeneously distributed as evidenced by the darkly imaged STEM-HAADF image (Fig. 5c). On this image, precipitates clearly appear inside of a deformation band, indicating that they were not dissolved locally, which is also confirmed by the SAED pattern (inset bottom left on Fig. 5d). Shear localization has already been reported in ordered compounds deformed by SPD at a relatively low strain rate [15] or high temperature [16], or in hardened Ni-based alloys [17]. It is usually connected to local dynamic recrystallization, and leads to grain refinement. However, the mechanisms involved during SPD are quite different, since precipitates are not dissolved.

To summarize our experimental results, a schematic representation of microstructure evolution during SPD is given in Fig. 6, where the influence of Be in solid solution in fcc Cu is compared with that of a high density of nanoscaled  $\gamma$ -CuBe precipitates. Applying large strain in quasi-hydrostatic conditions (HPT) to a solubilized alloy (Fig. 6a) leads to a dramatic increase in the dislocation density and classical dynamic recovery, and the recrystallization mechanisms lead to grain refinement after unloading [4]. However, the achieved grain size is much smaller than that in pure Cu due to the strong interaction of Be with crystalline defects, which slows down recovery mechanisms [3].

If dislocation nucleation and glide are assumed to be a deformation energy dissipation mechanism and their originating phenomenon are used for further grain refinement, one can expect that hindering dislocations mobility can significantly change strain accommodation mechanisms in materials. Such effect can be clearly observed in the precipitation-hardened Cu-Be system, since dislocations pinning by nanoprecipitate particles leads to considerable strengthening, even in a coarse-grained state, due to higher yield stress. At the applied large strain in quasi-hydrostatic conditions (Fig. 6b), these  $\gamma$ -CuBe precipitates with theoretical hardness of 1000 HV [3] are too stiff to be

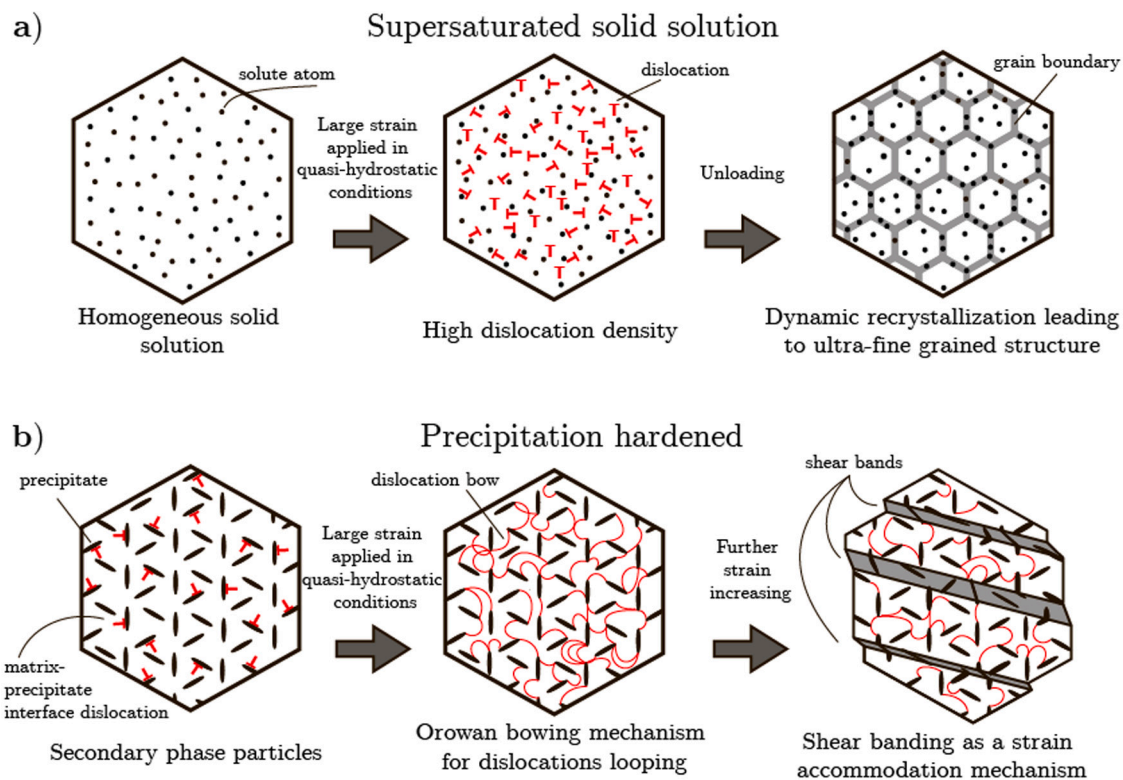


**Fig. 6.** Schematic representation of the microstructure evolution stages in solubilized (a) and precipitation-hardened (b) Cu-2Be alloy during the application of large strain by severe plastic deformation.

sheared during deformation at relatively low strain rates, thus, dislocations mobility most likely appear in the matrix while deforming the alloy. Misfit of lattices (Fig. 2) leads the precipitate–matrix interface to emit dislocations, providing their looping as an outcome of Orowan mechanisms. Due to the high density of precipitates and the fact that their hardness makes them unable to efficiently accommodate dislocations, dislocation density in the surrounding Cu matrix increases dramatically. In a classical tensile test at a critical strain value, the main energy draining mechanism would leave a loop around the by-passed precipitates, giving rise to a strain hardening and hence providing uniform elongation [18] with further fracture as a mechanical energy accommodation mechanism (Fig. 1a). However, under the applied high hydrostatic pressure, fracture is hindered since the high hydrostatic pressure under HPT conditions (6 GPa) inhibits damage. In order to minimize total energy and decrease dislocation density in such conditions, local high stress creates twisted (rotated) regions. Shear bands appear in the direction governed by crystallographic orientation of the copper matrix in a certain grain. This can be clearly seen from SEM images, where shear bands traverse a single grain following crystallographic defects such as copper twins (Fig. 3d). Under this process, precipitates became weaker obstacles, and hence sheared. As soon as the plastic strain is localized in such shear bands, the mean dislocation density remains relatively stable and the conditions for dynamic recrystallization that lead to grain refinement are not fulfilled, at least for the range of plastic strains used in the present HPT experiments. The presence of this shear band affects further mechanical properties of the processed alloy. Boundaries of these shear bands seem to become additional obstacles for effective dislocation glide, and trap dislocations in a way similar to that for nano-twins boundaries [19]. This leads

to the observed insignificant increase in yield limit compared to the un-deformed precipitation-hardened alloy (Fig. 1a).

#### 4. Summary

In summary, this experimental work shows that when dislocation glide is strongly hindered by a high density of precipitates, large strains applied under high hydrostatic pressure may localize in shear bands. Such phenomenon occurs even at a relatively low strain rate, and thus is very different in nature from adiabatic shear band formation followed by complete precipitates dissolution reported for high strain rates [20] and precipitation-hardened alloys [21].

#### CRediT authorship contribution statement

**Ivan Lomakin:** Conceptualization, Formal analysis, Methodology, Investigation, Visualization, Data curation, Writing – original draft, Writing – review & editing. **Alfiia Nigmatullina:** Investigation, Validation, Writing – review & editing. **Xavier Sauvage:** Conceptualization, Methodology, Investigation, Data curation, Formal analysis, Writing – review & editing.

#### Declaration of competing interest

The authors declare that they have no known competing financial interests or personal relationships that could have appeared to influence the work reported in this paper.

#### Acknowledgments

Ivan Lomakin and Xavier Sauvage are grateful to the Embassy of France in Russia for supporting their collaboration through Mechanikov's Scholarship. This work was partially supported by Saint Petersburg State University, Russia via Lot 2017 applied (id: 26130576). This

work was partially supported by Academy of Finland through grant 317464. XRD results were obtained by the “Center for X-ray Diffraction Methods” of the Research park of Saint Petersburg University. Anvils for HPT tool were produced in collaboration with center “Applied aerodynamics” of the Research park of Saint Petersburg University. Authors acknowledge the provision of facilities and technical support by Aalto University at OtaNano - Nanomicroscopy Center (Aalto-NMC).

## References

- [1] E. Orowan, Zur kristallplastizität. III. Über den mechanismus des gleitvorganges, *Z. Phys.* 89 (1934) 634.
- [2] M. Polanyi, Über eine art gitterstörung, die einen kristall plastisch machen könnte, *Z. Phys.* 89 (1934) 660, <http://dx.doi.org/10.1007/BF01341481>.
- [3] I. Lomakin, M. Castillo-Rodríguez, X. Sauvage, Microstructure, mechanical properties and aging behaviour of nanocrystalline copper - beryllium alloy, *Mater. Sci. Eng. A* 744 (2019) 206–214.
- [4] R. Valiev, R. Islamgaliev, I. Alexandrov, Bulk nanostructured materials from severe plastic deformation, *Prog. Mater. Sci.* 45 (2) (2000) 103–189, [http://dx.doi.org/10.1016/S0079-6425\(99\)00007-9](http://dx.doi.org/10.1016/S0079-6425(99)00007-9), URL: <https://linkinghub.elsevier.com/retrieve/pii/S0079642599000079>.
- [5] W. Lefebvre, N. Masquelier, J. Houard, R. Patte, H. Zapolsky, Tracking the path of dislocations across ordered Al<sub>3</sub>Zr nano-precipitates in three dimensions, *Scr. Mater.* 70 (2014) 43–46, <http://dx.doi.org/10.1016/j.scriptamat.2013.09.014>, URL: <https://linkinghub.elsevier.com/retrieve/pii/S1359646213004697>.
- [6] K.S. Kormout, R. Pippan, A. Bachmaier, Deformation-induced supersaturation in immiscible material systems during high-pressure torsion, *Adv. Energy Mater.* 19 (4) (2017) 1600675, <http://dx.doi.org/10.1002/adem.201600675>, URL: <http://doi.wiley.com/10.1002/adem.201600675>.
- [7] K. Edalati, R. Uehiro, K. Fujiwara, Y. Ikeda, H.-W. Li, X. Sauvage, R.Z. Valiev, E. Akiba, I. Tanaka, Z. Horita, Ultra-severe plastic deformation: Evolution of microstructure, phase transformation and hardness in immiscible magnesium-based systems, *Mater. Sci. Eng. A* 701 (2017) 158–166, <http://dx.doi.org/10.1016/j.msea.2017.06.076>, URL: <https://linkinghub.elsevier.com/retrieve/pii/S0921509317308432>.
- [8] I.V. Lomakin, A.R. Arutyunyan, R.R. Valiev, F.A. Gadzhiev, M.Y. Murashkin, Design and evaluation of an experimental technique for mechanical and fatigue testing of sub-sized samples, *Exp. Tech.* 42 (3) (2018) 261–270, <http://dx.doi.org/10.1007/s40799-017-0229-7>, URL: <http://link.springer.com/10.1007/s40799-017-0229-7>.
- [9] S.V. Franklin, F. Mertens, M. Marder, Portevin - le chatelier effect, *Phys. Rev. E* 62 (6) (2000) 8195–8206, <http://dx.doi.org/10.1103/PhysRevE.62.8195>, URL: <https://link.aps.org/doi/10.1103/PhysRevE.62.8195>.
- [10] P. Frint, M.F.-X. Wagner, Strain partitioning by recurrent shear localization during equal-channel angular pressing of an AA6060 aluminum alloy, *Acta Mater.* 176 (2019) 306–317, <http://dx.doi.org/10.1016/j.actamat.2019.07.009>, URL: <https://www.sciencedirect.com/science/article/pii/S1359645419304392>.
- [11] T.D. Horn, C.B. Silberman, P. Frint, M.F.-X. Wagner, J. Ihlemann, Strain localization during equal-channel angular pressing analyzed by finite element simulations, *Metals* 8 (1) (2018) <http://dx.doi.org/10.3390/met8010055>, URL: <https://www.mdpi.com/2075-4701/8/1/55>.
- [12] H. Tsubakino, R. Nozato, A. Yamamoto, Precipitation sequence for simultaneous continuous and discontinuous modes in Cu - Be binary alloys, *Mater. Sci. Technol.* 9 (4) (1993) 288–294, <http://dx.doi.org/10.1179/026708393790172097>, URL: [http://openurl.ingenta.com/content/xref?genre=article\(&issn=0267-0836&volume=9&issue=4&spage=288](http://openurl.ingenta.com/content/xref?genre=article(&issn=0267-0836&volume=9&issue=4&spage=288).
- [13] K. Shimizu, Y. Mikami, H. Mitani, K. Otsuka, Electron microscopy study of the precipitation processes in Cu - 2 wt.% Be alloy, *Trans. Jpn. Inst. Metals* 12 (3) (1971) 206–213, <http://dx.doi.org/10.2320/matertrans1960.12.206>, URL: [https://www.jstage.jst.go.jp/article/matertrans1960.12/3/12/206/\\_article](https://www.jstage.jst.go.jp/article/matertrans1960.12/3/12/206/_article).
- [14] S. Yamamoto, M. Matsui, Y. Murakami, Electron microscopic observation on the precipitation sequence in Cu - 2 wt.% Be alloy, *Trans. Jpn. Inst. Metals* 12 (3) (1971) 159–165, <http://dx.doi.org/10.2320/matertrans1960.12.159>, URL: [https://www.jstage.jst.go.jp/article/matertrans1960.12/3/12/159/\\_article](https://www.jstage.jst.go.jp/article/matertrans1960.12/3/12/159/_article).
- [15] C. Rentenberger, H. Karthaler, On the evolution of a deformation induced nanostructure in a Ni<sub>3</sub>Al alloy, *Acta Mater.* 53 (10) (2005) 3031–3040, <http://dx.doi.org/10.1016/j.actamat.2005.03.016>, URL: <https://linkinghub.elsevier.com/retrieve/pii/S1359645405001643>.
- [16] G.G. Maier, E.G. Astafurova, A comparison of strengthening mechanisms of austenitic Fe-13Mn-1.3C steel in warm and cold high-pressure torsion, *Metals* 10 (4) (2020) URL: <https://www.mdpi.com/2075-4701/10/4/493>.
- [17] P.C. Yadav, S. Sahu, A. Subramaniam, S. Shekhar, Effect of heat-treatment on microstructural evolution and mechanical behaviour of severely deformed Inconel 718, *Mater. Sci. Eng. A* 715 (2018) 295–306, <http://dx.doi.org/10.1016/j.msea.2018.01.007>, URL: <https://linkinghub.elsevier.com/retrieve/pii/S0921509318300078>.
- [18] T. Gladman, Precipitation hardening in metals, *Mater. Sci. Technol.* 15 (1) (1999) 30–36, <http://dx.doi.org/10.1179/026708399773002782>.
- [19] R. Islamgaliev, R. Valiev, R. Mishra, A. Mukherjee, Enhanced superplastic properties in bulk metastable nanostructured alloys, *Mater. Sci. Eng. A* 304–306 (2001) 206–210, [http://dx.doi.org/10.1016/S0921-5093\(00\)01440-4](http://dx.doi.org/10.1016/S0921-5093(00)01440-4), URL: <https://linkinghub.elsevier.com/retrieve/pii/S0921509300014404>.
- [20] H. Zhan, W. Zeng, G. Wang, D. Kent, M. Dargusch, Microstructural characteristics of adiabatic shear localization in a metastable beta titanium alloy deformed at high strain rate and elevated temperatures, *Mater. Charact.* 102 (2015) 103–113, <http://dx.doi.org/10.1016/j.matchar.2015.02.017>, URL: <https://linkinghub.elsevier.com/retrieve/pii/S1044580315000546>.
- [21] M.H. Colliander, G. Sundell, M. Thuvander, Complete precipitate dissolution during adiabatic shear localisation in a Ni-based superalloy, *Phil. Mag. Lett.* 100 (12) (2020) 561–570, <http://dx.doi.org/10.1080/09500839.2020.1820595>.